IEEE Access
Multidisciplinary | Rapid Review | Open Access Journal

Received August 6, 2019, accepted August 29, 2019, date of publication September 3, 2019, date of current version September 25, 2019.

Digital Object Identifier 10.1109/ACCESS.2019.2939257

Mathematical Modeling and Characteristics Analysis of the Toroidal Drive With Elastic Deformation in the Conjugating Process

XUELIAN ZENG[1,2], LIGANG YAO[1], JUN ZHANG[1], GUIYONG GUO[1], AND MEI HONG[1]
[1]School of Mechanical Engineering and Automation, Fuzhou University, Fuzhou 350108, China
[2]Department of Automobile Application Engineering, Fujian Chuanzheng Communications College, Fuzhou 350007, China

Corresponding authors: Ligang Yao (ylgyao@fzu.edu.cn) and Jun Zhang (zhang_jun@tju.edu.cn)

This work was supported in part by the Natural Science Foundation of China under Grant 50675035, Grant 51275092, and Grant 51505085, and in part by the Fujian Provincial Industrial Robot Basic Components Technology Research and Development Center under Grant 2014H21010011.

ABSTRACT Time-variation of meshing stiffness is the main internal excitation for the vibration and noise of the gear transmission system. Elastic deformation in the rolling contact process is an important factor for the meshing stiffness variation of the toroidal drive. However, most of the previous meshing modeling of the toroidal drive is based on the rigidity hypothesis. In order to investigate the actual contact situation and improve the stability of the toroidal drive, this paper focuses on the mathematical modelling and characteristics analysis for the toroidal drive with elastic deformation in the conjugating process between the planet-worm gear and sun-worm as well as between the planet-worm gear and internal toroidal gear. The elastic deformation integrated coordinate system of the toroidal drive is introduced. The elastic deformation velocity induced by contact force is adopted for the first time in the relative velocity of the Wills law for the toroidal drive. Then, based on Hertz contact theory, the relationship between elastic deformation velocity and normal force is studied. In addition, the influences of the elastic deformation on the meshing contact curve, helix-lead angle and induced normal curvature are further discussed.

INDEX TERMS Toroidal drive, elastic deformation, mathematical modeling, conjugating process.

I. INTRODUCTION

The toroidal drive was proposed by Kuehnle in 1966 [1]. As shown in Fig. 1, the drive is composed of a central input sun-worm, a stationary internal toroidal gear, a central output planet carrier and planet worm-gears with a number of meshing rollers. Compact structure, high carrying capacity and smooth transmission are the advantages of toroidal drive. A lot of researches have been done on toroidal drive, including meshing theory [2], [3], load distributions [4], friction coefficient [5], wear calculation [6], manufacture [7], [8], and so on.

However, previous analytical models of the toroidal drive are based on rigid-body hypothesis and without considering elastic deformation. Actually, deformations inevitable occur on the contact surface under the action of load, which will induce the variation of mesh stiffness. Time variation of the meshing stiffness is one of the main internal excitations of the vibration and noise for the toroidal drive. Therefore, the study on elastic deformation in the rolling contact process of the toroidal is essential.

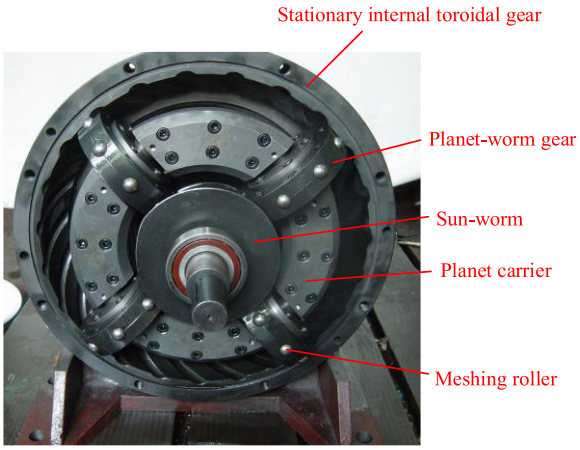

FIGURE 1. Schematic structure of a toroidal drive.

The researches on meshing stiffness and elastic deformation of other kind gear transmission system have always been

The associate editor coordinating the review of this manuscript and approving it for publication was Zhixiong Peter Li.

hot topics. Mo *et al*. [9] proposed a new calculation model, where the normal force acted on the teeth is calculated by the time-varying deformation of the meshing spring. The deformation was affected by the vibration displacement, installation error, tooth frequency error and eccentric error of the gear. Based on the thin slice assumption, Sun *et al*. [10] developed a revised time-varying mesh stiffness model of spur gear pairs with tooth modifications. The spur gear was divided into many individual slices along tooth width, and considering the revised fillet-foundation stiffness, the nonlinear contact stiffness, and the tooth profile errors, the stiffness of each slice gear pair was figured out. Cooley *et al.* [11] compared spur gear tooth mesh stiffness calculations by two approaches. In view of time-varying meshing stiffness, time-varying friction, load distribution, comprehensive transmission error and backlash, Shi *et al*. [12] established the dynamic model of a spur gear pair under multi-state meshing conditions such as teeth separation, drive- and back-side tooth mesh. The effects of load, backlash and comprehensive transmission error on meshing states and vibro-impact properties of the system were studied by defining three different Poincaré maps. Ma *et al.* [13] put forward an improved analytical method suitable for gear pairs with tip relief to determine time-varying mesh stiffness. Based on the improved analytical model, time-varying mesh stiffness under different torques, lengths, and amounts of profile modification was compared with that obtained from analytical finite element approach. Wang *et al*. [14] established dynamic models considering time-varying stiffness, gear clearance, and friction. The stiffness and elastic deformation of gear teeth were calculated using the finite element method with actual geometry and gear positions. Lin and Cai [15] proposed a model for predicting the tooth elastic deformation of curve-face gear based on Buckingham's assumption and the concept of equivalent gear. Chen and Shao [16] coupled the ring deformation into the gear mesh stiffness model of the internal gear pair based on the uniformly distributed Timoshenko beam theory. Ajmi and Velex [17] presented a general approach to the simulation of deflections and load distributions on solid spur and helical gears. The numerical results indicated that gear body distortions were critical for both static and dynamic simulations. Chang *et al*. [18] and Sánchez *et al.* [19] established a model for determining the contact forces and deformations in spur gear transmissions with finite element method and local contact analysis of elastic bodies. The deformation at each contact point was separated into a linear global term and a nonlinear local contact term. Nakhatakyan [20] proposed an analytical method for determining the flexural stress concentration factor in gear teeth considering elastic deformations, manufacture and assembly errors. Deduced the universal formulas for the flexural stress concentration factor in gear teeth. For studying the effects of multi-tooth contact as well as backlash and side contact of the multi-meshed geared systems, Eberhard [21] regarded the teeth and body of a gear as a rigid part, and the connection between them as an elastic part. Hu *et al*. [22] came to a conclusion through research that the gear meshing noise level in the compound planetary gear set can be decreased significantly by matching the engagement parameters, such as meshing stiffness, tooth error, and pitch error.

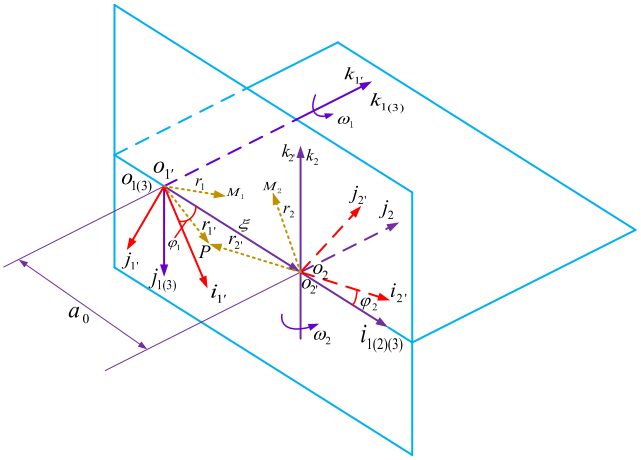

FIGURE 2. Coordinate systems of a toroidal drive integrated with elastic deformation.

In order to investigate the effect of elastic deformation on meshing performance in a toroidal drive, this paper proposes the meshing coordinate system with elastic deformation, creates a mathematical model of the toroidal drive with elastic deformation. Finally, based on the mathematical model, compares and analyses the meshing characteristic curves with elastic deformation and without elastic deformation.

II. ELASTIC DEFORMATION COORDINATE SYSTEM OF THE TOROIDAL DRIVE

To expound the position relationship among the main components of the toroidal drive, the coordinate system should be established first. Integrated with elastic deformation, the coordinate system of a toroidal drive is shown in Fig. 2. Three sets of coordinate systems, denoted by subscripts 1, 2 and 3 are given to describe the sun-worm, planet-worm gear and stationary internal toroidal gear, respectively.

The coordinate systems $\mathbf{S}_1(O_1, \boldsymbol{i}_1, \boldsymbol{j}_1, \boldsymbol{k}_1)$, $\mathbf{S}_2(O_2, \boldsymbol{i}_2, \boldsymbol{j}_2, \boldsymbol{k}_2)$ and $\mathbf{S}_3(O_3, \boldsymbol{i}_3, \boldsymbol{j}_3, \boldsymbol{k}_3)$ are the reference frames initially fixed at the centre of the sun-worm, planet-worm gear and internal toroidal gear, respectively. The body-fixed coordinate system $\mathbf{S}_{1'}(O_{1'}, \boldsymbol{i}_{1'}, \boldsymbol{j}_{1'}, \boldsymbol{k}_{1'})$ is embedded in the sum-worm gear and rotates with the sun-worm about axis $\boldsymbol{k}_{1'}$ with angular velocity $\boldsymbol{\omega}_1$ by angle $\boldsymbol{\varphi}_1$. Moving coordinate system $\mathbf{S}_{2'}(O_{2'}, \boldsymbol{i}_{2'}, \boldsymbol{j}_{2'}, \boldsymbol{k}_{2'})$ is rigidly connected to the planet-worm gear and rotates about axis $\boldsymbol{k}_{2'}$ by angle $\boldsymbol{\varphi}_2$ with angular velocity $\boldsymbol{\omega}_2$. $\sum(1)$, $\sum(2)$, $\sum(3)$ respectively represent the tooth surface of sun-worm, planet-worm gear and stationary internal toroidal gear. The origins $O_{1'}$ and $O_{2'}$ are respectively on the terminals of the vector ξ.

As shown in Fig. 3, the coordinate system $\mathbf{S}_0(O_0, \boldsymbol{i}_0, \boldsymbol{j}_0, \boldsymbol{k}_0)$ is the reference frame of the roller and $\mathbf{S}_{0'}(O_{0'}, \boldsymbol{i}_{0'}, \boldsymbol{j}_{0'}, \boldsymbol{k}_{0'})$ is the movable coordinate system rigidly connected to the centre of a roller.

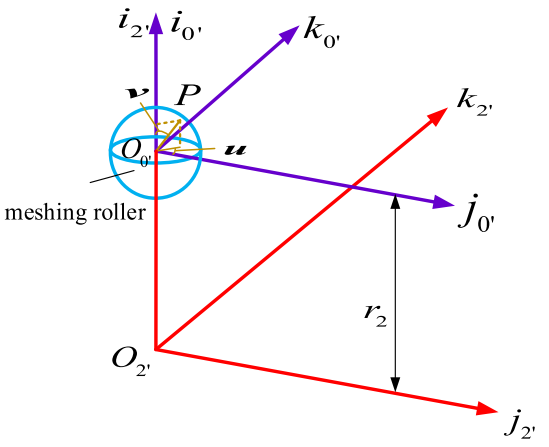

FIGURE 3. Elastic deformation coordinate system between the meshing roller and planet-worm gear.

III. ELASTIC MESHING EQUATIONS OF THE TOROIDAL DRIVE

In order to reveal the actual working situation of a toroidal drive, this work includes the elastic deformation caused by contact force in the meshing equation. After analyzing the contact relationship between the sun-worm tooth surface and rollers, the normal force at contact point is analyzed. Then, the formulas of elastic deformation as well as relative velocity at contact point of the toroidal drive are deduced according to Wills law and differential geometry theory.

A. CONJUGATE ELASTIC MESHING EQUATIONS

Assuming P is the elastic meshing contact point on the surface of the meshing roller, as shown in Fig. 2. The equation of point P in $\mathbf{S}_{2'}$ can be denoted as:

$$\boldsymbol{r}_{2'} = [x_{2'}, y_{2'}, z_{2'}]^{\mathrm{T}} = \boldsymbol{M}_{2'0} \cdot \boldsymbol{r}_0 = \begin{bmatrix} \rho\cos v + r_2 \\ \rho\cos u\sin v \\ \rho\sin u\sin v \end{bmatrix} \tag{1}$$

where $\boldsymbol{r}_{2'}$ is the vector of meshing roller in $\mathbf{S}_{2'}$. $\boldsymbol{M}_{2'0}$ is the coordinate transformation matrix from $\mathbf{S}_0$ to $\mathbf{S}_{2'}$. $\boldsymbol{r}_0$ is the vector of meshing roller in $\mathbf{S}_0$, ρ is the radius of meshing roller. r_2 is the radius of the planet-worm gear. u and v are spherical parameters of meshing roller.

As shown in fig. 2, assume that when the sun-worm and planet-worm gear respectively rotate $\boldsymbol{\varphi}_1$ and $\boldsymbol{\varphi}_2$, the initial position of the sun-worm tooth surface $\sum(1)$ and the planet-worm gear tooth surface $\sum(2)$ will arrive at point P simultaneously from point M_1 and point M_2. $\boldsymbol{r}_1$, $\boldsymbol{r}_2$ respectively represent the radius vectors O_1M_1 and O_2M_2. $\boldsymbol{r}_{1'}$, $\boldsymbol{r}_{2'}$ respectively represent the radius vectors $O_{1'}P$ and $O_{2'}P$.

Based on Wills law [23], the elastic meshing equation and elastic meshing function in $\mathbf{S}_{2'}$ of two conjugate surfaces, $\sum(1)$ and $\sum(2)$, can be represented as:

$$\boldsymbol{n}_{2'} \cdot \boldsymbol{v}^{(2'1')} = 0 \tag{2}$$

$$\Phi = \boldsymbol{n}_{2'} \cdot \boldsymbol{v}^{(2'1')} \tag{3}$$

where vector $\boldsymbol{n}_{2'}$ is the unit normal vector of contact point P in $\mathbf{S}_{2'}$ system. Vector $\boldsymbol{v}^{(2'1')}$ is the relative velocity between the planet-worm gear and sun-worm at contact point P. In this paper, we assume that the elastic deformation at the contact point does not change the direction of the common normal, and the flexural deformation is too small to affect the common normal line. Therefore, the correction of vector $\boldsymbol{n}_{2'}$ is unnecessary. Vector $\boldsymbol{n}_{2'}$ in $\mathbf{S}_{2'}$ can be represented as:

$$\boldsymbol{n}_{2'} = \frac{\boldsymbol{N}_{2'}}{|\boldsymbol{N}_{2'}|} = \begin{bmatrix} \cos v \\ \cos u\sin v \\ \sin u\sin v \\ 1 \end{bmatrix} \tag{4}$$

where,

$$\begin{aligned} \boldsymbol{N}_{2'} &= \frac{\partial \boldsymbol{r}_{2'}}{\partial u} \times \frac{\partial \boldsymbol{r}_{2'}}{\partial v} \\ &= \begin{bmatrix} 0 & -\frac{\partial z_{2'}}{\partial u} & \frac{\partial y_{2'}}{\partial u} & 0 \\ \frac{\partial z_{2'}}{\partial u} & 0 & -\frac{\partial x_{2'}}{\partial u} & 0 \\ -\frac{\partial y_{2'}}{\partial u} & \frac{\partial x_{2'}}{\partial u} & 0 & 0 \\ 0 & 0 & 0 & 1 \end{bmatrix} \begin{bmatrix} \frac{\partial x_{2'}}{\partial v} \\ \frac{\partial y_{2'}}{\partial v} \\ \frac{\partial z_{2'}}{\partial v} \\ 1 \end{bmatrix} \end{aligned} \tag{5}$$

Assume that the direction and magnitude of $\boldsymbol{\omega}_1$ and that of $\boldsymbol{\omega}_2$ are determined, as the transmission ratio formula between a planet-worm gear and the sun-worm is $|\boldsymbol{i}_{21}| = |\boldsymbol{\omega}_{2'}\ \boldsymbol{\omega}_1| = |\boldsymbol{\varphi}_2/\boldsymbol{\varphi}_1|$, setting $|\boldsymbol{\omega}_1| = 1$ will yield $|\boldsymbol{\omega}_2| = |\boldsymbol{i}_{21}|$. Based on Wills law, the relative velocity vector $\boldsymbol{v}^{(2'1')}$ at point P can be represented as follows:

$$\boldsymbol{v}^{(2'1')} = \boldsymbol{\omega}^{(2'1')} \times \boldsymbol{r}_{2'} - \boldsymbol{\omega}_1 \times \boldsymbol{\xi} + \frac{\mathrm{d}\boldsymbol{\xi}}{\mathrm{d}t} + \frac{d\boldsymbol{\delta}^{(2'1')}}{dt} + \frac{d\boldsymbol{\delta}_{\xi}^{(2'1')}}{dt} \tag{6}$$

where $\boldsymbol{\omega}^{(2'1')}$ is the relative angular velocity between the planet-worm gear and sun-worm. $\boldsymbol{\xi}$ is the central-distance in $\mathbf{S}_1$ and can be described as:

$$\boldsymbol{\xi} = \overrightarrow{\boldsymbol{o}_{1'}\boldsymbol{o}_{2'}} = a_0\boldsymbol{i}_1 \tag{7}$$

The following equations exist in $\mathbf{S}_{2'}$:

$$\begin{cases} \boldsymbol{\omega}_2 = \boldsymbol{\omega}_2\boldsymbol{k}_{2'} = i_{21}\boldsymbol{k}_{2'} \\ \boldsymbol{\omega}_1 = \boldsymbol{k}_{1'} = \sin\varphi_2\boldsymbol{i}_{2'} + \cos\varphi_2\boldsymbol{j}_{2'} \\ \boldsymbol{\omega}^{(2'1')} = \boldsymbol{\omega}_2 - \boldsymbol{\omega}_1 = -\sin\varphi_2\boldsymbol{i}_{2'} - \cos\varphi_2\boldsymbol{j}_{2'} + i_{21}\boldsymbol{k}_{2'} \\ \boldsymbol{\omega}^{(2'1')} \times \boldsymbol{r}_{2'} \\ = \begin{bmatrix} 0 & -i_{21} & -\cos\varphi_2 & 0 \\ i_{21} & 0 & \sin\varphi_2 & 0 \\ \cos\varphi_2 & -\sin\varphi_2 & 0 & 0 \\ 0 & 0 & 0 & 1 \end{bmatrix} \begin{bmatrix} x_{2'} \\ y_{2'} \\ z_{2'} \\ 1 \end{bmatrix} \end{cases} \tag{8}$$

As shown in Fig. 2, ξ can be transformed to $\mathbf{S}_{2'}$ via coordinate transformation matrix $\boldsymbol{M}_{2'1}$ and it can be represented in $\mathbf{S}_{2'}$ as follows:

$$\boldsymbol{\xi} = \begin{bmatrix} a_0\cos\varphi_2 \\ -a_0\sin\varphi_2 \\ 0 \\ 1 \end{bmatrix} \tag{9}$$

There is no relative movement between the rotation centre of the sun-worm $O_{1'}$ and the rotation centre of the planet worm-gear $O_{2'}$, then it can be obtained: $d\xi/dt = 0$.

The fifth term of Eq. (6) $d\,\delta_{\xi}^{(2'1')}/dt$ is the elastic deformation velocity along the direction of $O_{1'}O_{2'}$. Because coordinate systems $\mathbf{S}_{1'}$ and $\mathbf{S}_{2'}$ are fixed at the centre of the rotating axes of the sun-worm and planet-worm gear, and the distance of two rotating origins $O_{1'}$ and $O_{2'}$ is constant, we can obtain $d\,\delta_{\xi}^{(2'1')}/dt = 0$.

Therefore, the relative velocity vector $\boldsymbol{v}^{(2'1')}$ can be represented as:

$$\boldsymbol{v}^{(2'1')} = \boldsymbol{\omega}^{(2'1')} \times \boldsymbol{r}_{2'} - \boldsymbol{\omega}_1 \times \boldsymbol{\xi} + \frac{d\boldsymbol{\delta}^{(2'1')}}{dt} \tag{10}$$

where $d\,\boldsymbol{\delta}^{(2'1')}/dt$ is the elastic deformation velocity along the translocation direction of the contact surface between the sun-worm and planet-worm gear, and induced by contact force $\boldsymbol{P}_1$ at meshing contact point P.

$\boldsymbol{v}^{(2'1')}$ can be obtained by calculation:

$$\boldsymbol{v}^{(2'1')} = \begin{bmatrix} -(i_{21}y_{2'} + \cos\varphi_2 z_{2'}) + \Delta v_{x2'} \\ i_{21}x_{2'} + \sin\varphi_2 z_{2'} + \Delta v_{y2'} \\ \cos\varphi_2 x_{2'} - \sin\varphi_2 y_{2'} + \Delta v_{z2'} \\ 1 \end{bmatrix} \tag{11}$$

where,

$$\frac{d\boldsymbol{\delta}^{(2'1')}}{dt} = \left[\Delta v_{x2'}, \Delta v_{y2'}, \Delta v_{z2'}\right]^T \tag{12}$$

$x_{2'}$, $y_{2'}$ and $z_{2'}$ are coordinate components of a roller motion profile in $\mathbf{S}_{2'}$. $\Delta\boldsymbol{v}_x 2'$, $\Delta\boldsymbol{v}_y 2'$ and $\Delta\boldsymbol{v}_z 2'$ are variations of the relative velocities at meshing contact point P of the conjugate surface between the meshing roller and sun-worm tooth profile.

The crucial problem is the analysis of the contact relationships between the sun-worm tooth and meshing roller, as well as between the stationary internal toroidal gear and meshing roller. In the following sections, taking the contact relationship between the sun-worm tooth and meshing rollers as an example, the relative velocity with elastic contact, as well as the mathematical model of the toroidal drive with elastic deformation will be discussed.

B. CONTACT RELATIONSHIP BETWEEN THE SUN-WORM TOOTH AND ROLLERS

The elastic contact between the sun-worm tooth and roller can be considered to be the contact between two free-form elastic bodies. The difference is that the principal curvatures in the principal planes does not equal to each other. The sun-worm tooth and roller contact with each other at point P under the action of normal force $\boldsymbol{P}_1$. As shown in Fig. 4 and Fig. 5, there are two principal planes of the sun-worm at point P. The 1st principal plane is through the normal line and the section of the sun-worm tooth. The 2nd principal plane is through the normal line and perpendicular to the 1st principal plane. According to the Hertz contact theory,

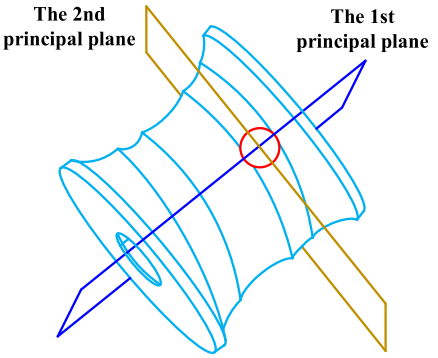

FIGURE 4. Principal planes of the sun-worm tooth and meshing roller.

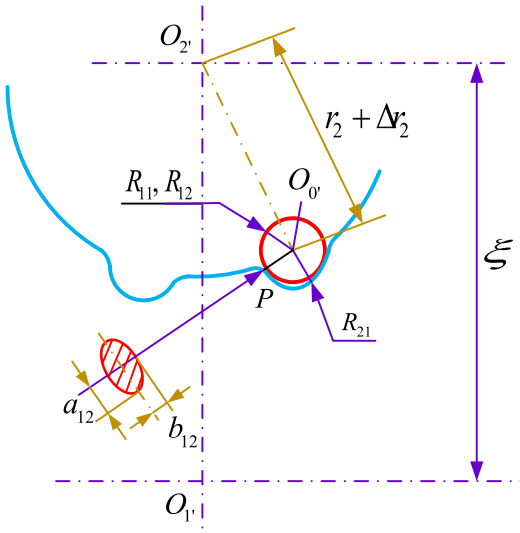

FIGURE 5. Contact relationships between the sun-worm tooth and meshing roller.

the contact point P becomes a small elliptical area due to the elastic deformation induced by the normal contact force $\boldsymbol{P}_1$ between the sun-worm tooth and meshing roller, as shown in Fig. 5.

C. PRINCIPAL CURVATURES OF THE SUN-WORM TOOTH AND MESHING ROLLER AT POINT P

The two principal planes of the sun-worm at point P are shown in Fig. 6(a) and (b). In the 1st principal plane, the contact condition of a meshing roller with the sun-worm tooth is similar to that of a spherical with a concave surface, and the curvature radius of the sun-worm is negative. In the 2nd principal plane, the contact condition of a meshing roller with the sun-worm tooth is similar to that of a spherical with a convex surface.

The curvature radius of the roller is ρ. Based on the calculation formulas of the principal curvature, the principal curvature equation of the sun-worm at point P is:

$$(EG - F^2)k_n^2 - (EN - 2FM + GL)k_n + (LN - M^2) = 0 \tag{13}$$

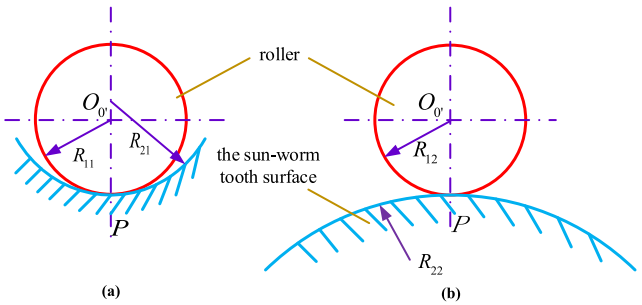

FIGURE 6. (a). First principal plane of the sun-worm tooth at point P. (b). Second principal plane of the sun-worm tooth at point P.

where,

$$\begin{cases} E = \boldsymbol{r}_{1'u}^2,\ F = \boldsymbol{r}_{1'u} \cdot \boldsymbol{r}_{1'v},\ G = \boldsymbol{r}_{1'v}^2 \\ L = \boldsymbol{n}_{2'} \cdot \boldsymbol{r}_{1'uu},\ M = \boldsymbol{n}_{2'} \cdot \boldsymbol{r}_{1'uv},\ N = \boldsymbol{n}_{2'} \cdot \boldsymbol{r}_{1'vv} \end{cases} \tag{14}$$

$$\boldsymbol{r}_{1'} = [l_1, l_2, l_3, 1]^T,\ \begin{cases} l_1 = \rho\cos v + r_2 - a_0\cos\varphi_2 \\ l_2 = \rho\cos u\sin v + a_0\sin\varphi_2 \\ l_3 = \rho\sin u\sin v \end{cases} \tag{15}$$

k_n can be obtained by calculation,

$$k_{n1} = \frac{-B - \sqrt{\Delta}}{2A},\quad k_{n2} = \frac{-B + \sqrt{\Delta}}{2A} \tag{16}$$

where,

$$\begin{cases} A = (EG - F^2) = \rho^4\sin^2 v(\cos^4 u + 2\sin^2 u\sin^2 v \\ \qquad - \cos^2 u\sin^2 u\cos^2 v) \\ B = -(EN - 2FM + GL) = \rho^3\sin^2 v(-3 + \cos^2 u \\ \qquad + 2\sin^2 u\cos^2 v + \cos^2 u) \\ C = LN - M^2 = \rho^2\sin^2 v \\ \Delta = B^2 - 4AC = \rho^6\sin^4 v(-4\sin^4 u\sin^2 v\cos^2 v \\ \qquad - 8\cos^2 u\sin v\cos v + 1) \end{cases} \tag{17}$$

According to the geometric relationship of Fig. 5 and Fig. 6, the curvatures of the sun-worm tooth and meshing roller at point P are:

$$\begin{cases} \rho_{11} = \rho_{12} = \dfrac{1}{\rho} \\ \rho_{21} = \dfrac{1}{R_{21}} = k_{n1} = \dfrac{-B - \sqrt{\Delta}}{2A} \\ \rho_{22} = \dfrac{1}{R_{22}} = k_{n2} = \dfrac{-B + \sqrt{\Delta}}{2A} \end{cases} \tag{18}$$

D. NORMAL FORCE P_1 AT THE CONTACT POINT P

The normal force acting on the contact region can be simplified as $\boldsymbol{P}_1$, which acts at the centre of the contact ellipse. The action line of $\boldsymbol{P}_1$ is in the normal plane that contains contact point P. As shown in Fig. 7(a) and (b), $\boldsymbol{r}_P$ is the radius vector of the sun-worm at meshing point P. In coordinate system $\mathbf{S}_{2'}$, $\boldsymbol{r}_P$ is equal to vector $\boldsymbol{r}_{1'}$.

Assume that the driving force between the sun-worm and planet-worm gear is $\boldsymbol{F}_{t1}$, the axial force and radial force are $\boldsymbol{F}_{a1}$ and $\boldsymbol{F}_{r1}$ respectively, as shown in Fig. 8. They all act on the pitch circle of the sun-worm. As shown in Fig. 9,

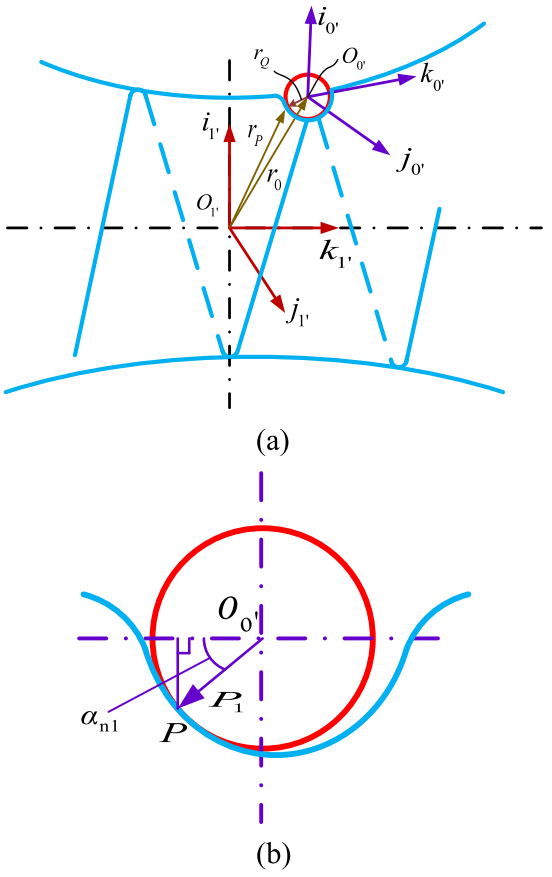

FIGURE 7. (a). Contact geometry model of the sun-worm tooth. (b). Normal force at point P.

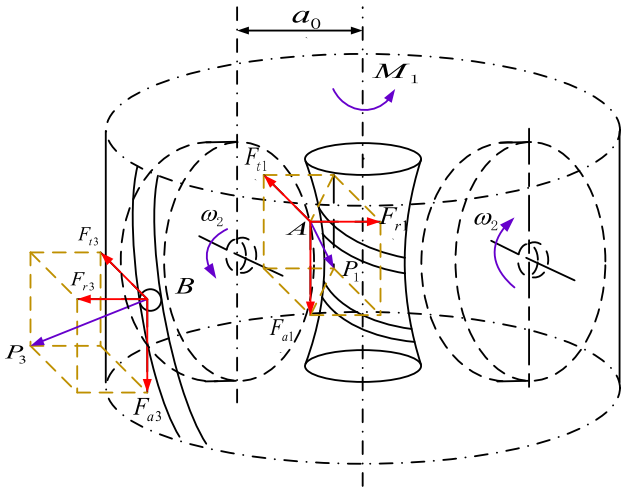

FIGURE 8. Force analysis of the sun-worm and stationary internal toroidal gear.

the magnitude of the reaction force $\boldsymbol{F}'_{t1}$, $\boldsymbol{F}'_{a1}$ and $\boldsymbol{F}'_{r1}$ are equal to the force $\boldsymbol{F}_{t1}$, $\boldsymbol{F}_{a1}$ and $\boldsymbol{F}_{r1}$ respectively, but with the opposite directions.

The torque of the sun-worm is $\boldsymbol{M}_1$. The module and unit vector of normal force $\boldsymbol{P}_1$ are P_1 and $\boldsymbol{n}_{2'}$, respectively. The meshing point number between the sun-worm and planet-

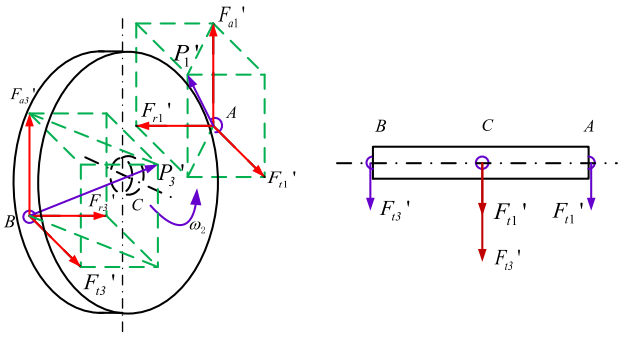

FIGURE 9. Force analysis of the planet-worm gear.

worm gears is m, and that between the stationary internal toroidal gear and planet-worm gear is n. k planet-worm gears are evenly distributed on the planet-carrier.

The following formula is available.

$$\begin{aligned}\boldsymbol{M}_1 &= k \cdot m \cdot (\boldsymbol{k}_{1'} \times \boldsymbol{r}_{\mathrm{p}}) \cdot \boldsymbol{P}_1 = k \cdot m \cdot (\boldsymbol{k}_{1'} \times \boldsymbol{r}_{\mathrm{p}}) \cdot (P_1 \boldsymbol{n}_{2'}) \\ &= k \cdot m \cdot P_1 \cdot (\boldsymbol{k}_{1'} \times \boldsymbol{r}_{\mathrm{p}}) \cdot \boldsymbol{n}_{2'} \end{aligned} \tag{19}$$

where,

$$\begin{cases} P_1 = \dfrac{\boldsymbol{M}_1}{k \cdot m \cdot (\boldsymbol{k}_{1'} \times \boldsymbol{r}_{\mathrm{P}}) \cdot \boldsymbol{n}_{2'}} \\ \boldsymbol{n}_{2'} = [n_{x2'}, n_{y2'}, n_{z2'}, 1]^{\mathrm{T}} = \begin{bmatrix} \cos v \\ \cos u \sin v \\ \sin u \sin v \\ 1 \end{bmatrix} = \begin{bmatrix} l_4 \\ l_5 \\ l_6 \\ 1 \end{bmatrix} \\ \boldsymbol{k}_{1'} = \sin\varphi_2 \mathrm{i}_{2'} + \cos\varphi_2 \mathrm{j}_{2'} \\ (\boldsymbol{k}_{1'} \times \boldsymbol{r}_{\mathrm{P}}) \cdot \boldsymbol{n}_{2'} = \boldsymbol{k}_{1'} \cdot (\boldsymbol{r}_{\mathrm{P}} \times \boldsymbol{n}_{2'}) \\ \quad = \begin{vmatrix} \sin\varphi_2 & \cos\varphi_2 & 0 \\ l_1 & l_2 & l_3 \\ l_4 & l_5 & l_6 \end{vmatrix} = R \end{cases} \tag{20}$$

Then P_1 can be obtained.

$$P_1 = \frac{\boldsymbol{M}_1}{k \cdot m \cdot R} \tag{21}$$

where,

$$\begin{aligned} R &= l_2 \cdot l_6 \sin\varphi_2 + l_3 \cdot l_4 \cos\varphi_2 - l_3 \cdot l_5 \sin\varphi_2 - l_1 \cdot l_6 \cos\varphi_2 \\ &= a_0 \sin u \sin v - r_2 \cos\varphi_2 \sin u \sin v \end{aligned} \tag{22}$$

E. EXPRESION OF $du/d\varphi_2$ AND $dv/d\varphi_2$

The meshing equation and the meshing function without elastic deformation can be obtained as:

$$\begin{cases} \sin(\alpha + u) = \dfrac{-l_8 \cos v}{\sqrt{l_9^2 + l_{10}^2 \sin v}} \\ \Phi_{21} = \boldsymbol{n}_{2'} \cdot \boldsymbol{v}^{(2'1')} = l_8 \cos v + l_9 \cos u \sin v + l_{10} \sin u \sin v \end{cases} \tag{23}$$

where,

$$\begin{cases} l_8 = 0, l_9 = i_{21} \cdot r_2, \quad l_{10} = r_2 \cos\varphi_2 + a_0 \\ \alpha = \tan^{-1}(l_9 / l_{10}) \end{cases} \tag{24}$$

Set $\boldsymbol{\Phi} = l_8 \cos v + C_u \cdot l_9 \sin v + S_u \cdot l_{10} \sin v = 0$.

C_u and S_u are regarded as constants. The expression of $dv/d\varphi_2$ can be represented as follows:

$$\frac{dv}{d\varphi_2} = \frac{l_{8'} \cos v + C_u \cdot l_{9'} \sin v + S_u \cdot l_{10'} \sin v}{-l_8 \sin v + C_u \cdot l_9 \cos v + S_u \cdot l_{10} \cos v} = \frac{l_{11}}{l_{12}} \tag{25}$$

where,

$$\begin{cases} l_{8'} = dl_8 / d\varphi_2 = 0 \\ l_{9'} = dl_9 / d\varphi_2 = 0 \\ l_{10'} = dl_{10} / d\varphi_2 = -r_2 \sin\varphi \\ l_{11} = -S_u \cdot r_2 \sin\varphi_2 \sin v \\ l_{12} = -C_u \cdot i_{21} \cdot r_2 \cos v - S_u \cdot (r_2 \cos\varphi_2 + a_0) \cos v \end{cases} \tag{26}$$

Similarly, set $\boldsymbol{\Phi} = C_v l_8 + S_v \cdot l_9 \cos u + S_v \cdot l_{10} \sin u = 0$.

C_v and S_v are regarded as constants. The expression of $du/d\varphi_2$ can be represented as follows:

$$\frac{du}{d\varphi_2} = \frac{C_v \cdot l_{8'} + S_v \cdot l_{9'} \cos u + S_v \cdot l_{10'} \sin u}{-S_v \cdot l_9 \sin u + S_v \cdot l_{10} \cos u} = \frac{l_{13}}{l_{14}} \tag{27}$$

where,

$$\begin{cases} l_{13} = -S_v \cdot r_2 \sin\varphi_2 \sin u \\ l_{14} = S_v \cdot i_{21} \cdot r_2 \sin u - S_v \cdot (r_2 \cos\varphi_2 + a_0) \cos u \end{cases} \tag{28}$$

F. ELASTIC DEFORMATION $\delta^{(2'1')}$ BETWEEN THE SUN-WORM AND PLANET-WORM GEAR AT POINT P

Due to the elastic deformation induced by the action of normal contact force $\boldsymbol{P}_1$ between the sun-worm tooth and meshing roller, the meshing contact point P becomes a small elliptical area, as shown in Fig. 5 and Fig. 10. Assume that a_{12} is the value of the major half-axis of the elliptical contact region along the x axis and b_{12} is the value of the minor half-axis of the elliptical contact region along the y axis. The parameters of the elliptical contact region at the meshing contact point P are:

$$\begin{cases} a_{12} = \alpha_{12} \sqrt[3]{\dfrac{\boldsymbol{P}_1 m_{12}}{n_{12}}} \\ b_{12} = \beta_{12} \sqrt[3]{\dfrac{\boldsymbol{P}_1 m_{12}}{n_{12}}} \\ m_{12} = \dfrac{4}{\rho_{11} + \rho_{12} + \rho_{21} + \rho_{22}} = \dfrac{4A \cdot \rho}{2A - B \cdot \rho} \\ n_{12} = \dfrac{8}{3\left(\dfrac{1-\mu_1^2}{E_1} + \dfrac{1-\mu_2^2}{E_2}\right)} \end{cases} \tag{29}$$

where, α_{12} and β_{12} are both interpolation coefficients. m_{12} and n_{12} are both geometry parameters of the contact ellipse of the sun-worm tooth and meshing roller. μ_1 and μ_2 are Poisson's ratio of the materials of the sun-worm and roller, respectively. E_1 and E_2 are elastic moduli of the materials of the sun-worm and roller, respectively. The vector $\boldsymbol{P}_1$ is the normal force at point P. ρ_{11}, ρ_{12}, ρ_{21} and ρ_{22} are the curvatures of the contact point P.

$$\tau_{12} = \sqrt{\frac{(\rho_{11}-\rho_{12})^2 + 2(\rho_{11}-\rho_{12})(\rho_{21}-\rho_{22})\cos 2\psi_{12} + (\rho_{21}-\rho_{22})^2}{\rho_{11}+\rho_{12}+\rho_{21}+\rho_{22}}} = \sqrt{\frac{\Delta\cdot\rho}{2A^2 - AB\cdot\rho}} \tag{30}$$

As shown in Fig. 10, the angle $\bar{\psi}$ between the x_1 axis (the direction of 1^{st} principal plane) and x axis, is equal to 0. Ψ_{12} is the angle between the two axes x_1 and x_2 that separately denotes the directions of the two principal planes ($\Psi_{12} = 90°$). According to the following equation, the value of τ_{12} is not affected by the value of $\boldsymbol{\Psi}_{12}$ (30), as shown at the top of this page.

According to the result of τ_{12} above, the interpretation coefficients α_{12} and β_{12} can be obtained. The elliptic integral parameters J_{12} and J_{12}/α_{12} determined by the result of τ_{12} can be achieved. Thus, the major and minor half-axis of the contact ellipse a_{12} and b_{12} can also be obtained. Therefore, the elastic deformation at meshing contact point P of the sun-worm tooth and meshing roller can be represented as:

$$\boldsymbol{\delta}^{(2'1')} = \frac{3\boldsymbol{P}_1}{2\pi\cdot a_{12}}\left(\frac{1-\mu_1^2}{E_1} + \frac{1-\mu_2^2}{E_2}\right)J_{12} \tag{31}$$

The equation above can also be given as follows:

$$\begin{cases} \boldsymbol{\delta}^{(2'1')} = \dfrac{3\boldsymbol{P}_1}{2\pi\cdot a_{12}}\left(\dfrac{1-\mu_1^2}{E_1} + \dfrac{1-\mu_2^2}{E_2}\right)J_{12} \\ \qquad = l_7\cdot\sqrt[3]{\boldsymbol{P}_1^2} = \left[\boldsymbol{\delta}_{x2'}^{(2'1')}, \boldsymbol{\delta}_{y2'}^{(2'1')}, \boldsymbol{\delta}_{z2'}^{(2'1')}\right]^{\mathrm{T}} \\ \boldsymbol{P}_1 = P_1\cdot\boldsymbol{n}_{2'} = \begin{bmatrix} P_1\cdot\cos v \\ P_1\cdot\cos u\sin v \\ P_1\sin u\sin v \end{bmatrix} = \begin{bmatrix} P_1\cdot l_4 \\ P_1\cdot l_5 \\ P_1\cdot l_6 \end{bmatrix} \\ l_7 = \dfrac{4J_{12}}{\pi\cdot\alpha_{12}\cdot\sqrt[3]{m_{12}\cdot n_{12}^2}} \end{cases} \tag{32}$$

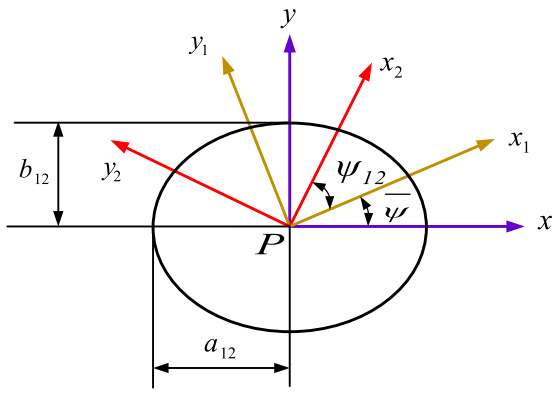

FIGURE 10. The contact coordinate system of the sun-worm tooth and meshing roller.

G. RELATIVE VELOCITY $\boldsymbol{v}^{(2'1')}$ BETWEEN THE SUN-WORM AND PLANET-WORM GEAR AT POINT P

According to the above analysis, taking the derivative of $\boldsymbol{\delta}^{(2'1')}$ (33), as shown at the top of the next page.

The final expression of the variation of the relative velocities at meshing contact point P of the conjugate surface between the meshing roller and sun-worm tooth profile can be represented as follows (34), as shown at the top of the next page.

where,

$$\begin{cases} \dfrac{dP_1}{dR} = \dfrac{-M_1}{k\cdot m\cdot R^2} \\ l_{Ru} = \dfrac{\partial R}{\partial u} = (a_0 - r_2\cos\varphi_2)\cos u\sin v \\ l_{Rv} = \dfrac{\partial R}{\partial v} = (a_0 - r_2\cos\varphi_2)\sin u\cos v \\ l_{4u} = \dfrac{\partial l_4}{\partial u} = 0\,, \quad l_{4v} = \dfrac{\partial l_4}{\partial v} = -\sin v \\ l_{5u} = \dfrac{\partial l_5}{\partial u} = -\sin u\sin v\,, \quad l_{5v} = \dfrac{\partial l_5}{\partial v} = \cos u\cos v \\ l_{6u} = \dfrac{\partial l_6}{\partial u} = \cos u\sin v\,, \quad l_{6v} = \dfrac{\partial l_6}{\partial v} = \sin u\cos v \end{cases} \tag{35}$$

Then, the relative velocity $\boldsymbol{v}^{(2'1')}$ with elastic deformation can be obtained.

IV. ELASTIC MESHING MODEL OF THE TOROIDAL DRIVE

According to the relative velocity expression deduced in part III, Elastic conjugate equations between the sun-worm and planet-worm gear as well as between the stationary internal toroidal gear and planet-worm gear can be obtained. In order to investigate the effect of elastic deformation on meshing performance, the equations of instantaneous contact curve, induced normal curvature and helix-lead angle of the toroidal drive that with elastic deformation are derived.

A. CONJUGATE EQUATION WITH ELASTIC DEFORMATION BETWEEN THE SUN-WORM AND PLANET-WORM GEAR

The elastic meshing model of conjugate surface $\sum(1)$ and $\sum(2)$ can be represented as follows:

$$i_{21}r_2\cos u\sin v + (r_2\cos\varphi_2 + a_0)\sin u\sin v + l_{21} = 0 \tag{36}$$

According to Eq. (36), the elastic meshing equation and elastic meshing function between the sun-worm and

$$\begin{cases} \Delta v_{x2'} = \dfrac{d\delta_{x2'}^{(2'1')}}{dt} = \dfrac{\partial \delta_{x2'}^{(2'1')}}{\partial P_1}\dfrac{dP_1}{dR}\left(\dfrac{\partial R}{\partial u}\dfrac{du}{d\varphi_2}\dfrac{d\varphi_2}{dt} + \dfrac{\partial R}{\partial v}\dfrac{dv}{d\varphi_2}\dfrac{d\varphi_2}{dt}\right) + \dfrac{\partial \delta_{x2'}^{(2'1')}}{\partial l_4}\left(\dfrac{\partial l_4}{\partial u}\dfrac{du}{d\varphi_2}\dfrac{d\varphi_2}{dt} + \dfrac{\partial l_4}{\partial v}\dfrac{dv}{d\varphi_2}\dfrac{d\varphi_2}{dt}\right) \\ \Delta v_{y2'} = \dfrac{d\delta_{y2'}^{(2'1')}}{dt} = \dfrac{\partial \delta_{y2'}^{(2'1')}}{\partial P_1}\dfrac{dP_1}{dR}\left(\dfrac{\partial R}{\partial u}\dfrac{du}{d\varphi_2}\dfrac{d\varphi_2}{dt} + \dfrac{\partial R}{\partial v}\dfrac{dv}{d\varphi_2}\dfrac{d\varphi_2}{dt}\right) + \dfrac{\partial \delta_{y2'}^{(2'1')}}{\partial l_5}\left(\dfrac{\partial l_5}{\partial u}\dfrac{du}{d\varphi_2}\dfrac{d\varphi_2}{dt} + \dfrac{\partial l_5}{\partial v}\dfrac{dv}{d\varphi_2}\dfrac{d\varphi_2}{dt}\right) \\ \Delta v_{z2'} = \dfrac{d\delta_{z2'}^{(2'1')}}{dt} = \dfrac{\partial \delta_{z2'}^{(2'1')}}{\partial P_1}\dfrac{dP_1}{dR}\left(\dfrac{\partial R}{\partial u}\dfrac{du}{d\varphi_2}\dfrac{d\varphi_2}{dt} + \dfrac{\partial R}{\partial v}\dfrac{dv}{d\varphi_2}\dfrac{d\varphi_2}{dt}\right) + \dfrac{\partial \delta_{z2'}^{(2'1')}}{\partial l_6}\left(\dfrac{\partial l_6}{\partial u}\dfrac{du}{d\varphi_2}\dfrac{d\varphi_2}{dt} + \dfrac{\partial l_6}{\partial v}\dfrac{dv}{d\varphi_2}\dfrac{d\varphi_2}{dt}\right) \end{cases} \tag{33}$$

$$\begin{cases} \Delta v_{x2'} = \dfrac{2i_{21}\cdot l_7}{3}\left[-\sqrt[3]{\dfrac{M_1^2 l_4^2}{k^2m^2R^5}}\left(\dfrac{l_{Ru}l_{13}}{l_{14}} + \dfrac{l_{Rv}l_{11}}{l_{12}}\right) + \sqrt[3]{\dfrac{M_1^2}{k^2m^2R^2l_4}}\left(\dfrac{l_{4u}l_{13}}{l_{14}} + \dfrac{l_{4v}l_{11}}{l_{12}}\right)\right] \\ \Delta v_{y2'} = \dfrac{2i_{21}\cdot l_7}{3}\left[-\sqrt[3]{\dfrac{M_1^2 l_5^2}{k^2m^2R^5}}\left(\dfrac{l_{Ru}l_{13}}{l_{14}} + \dfrac{l_{Rv}l_{11}}{l_{12}}\right) + \sqrt[3]{\dfrac{M_1^2}{k^2m^2R^2l_5}}\left(\dfrac{l_{5u}l_{13}}{l_{14}} + \dfrac{l_{5v}l_{11}}{l_{12}}\right)\right] \\ \Delta v_{z2'} = \dfrac{2i_{21}\cdot l_7}{3}\left[-\sqrt[3]{\dfrac{M_1^2 l_6^2}{k^2m^2R^5}}\left(\dfrac{l_{Ru}l_{13}}{l_{14}} + \dfrac{l_{Rv}l_{11}}{l_{12}}\right) + \sqrt[3]{\dfrac{M_1^2}{k^2m^2R^2l_6}}\left(\dfrac{l_{6u}l_{13}}{l_{14}} + \dfrac{l_{6v}l_{11}}{l_{12}}\right)\right] \end{cases} \tag{34}$$

planet-worm gear in $\mathbf{S}_{2'}$ can be represented as:

$$\begin{cases} \sin(\alpha + u) = \dfrac{-l_8\cos v - l_{21}}{\sqrt{l_9^2 + l_{10}^2}\sin v} \\ \boldsymbol{\Phi}_{21} = \boldsymbol{n}_{2'}\cdot\boldsymbol{v}^{(2'1')} = l_8\cos v + l_9\cos u\sin v \\ \qquad + l_{10}\sin u\sin v + l_{21} \end{cases} \tag{37}$$

where,

$$\begin{aligned} l_{21} &= \boldsymbol{n}_{2'}\cdot\frac{d\boldsymbol{\delta}^{(2'1')}}{dt} = l_4\cdot\Delta\boldsymbol{v}_{x2'} + l_5\cdot\Delta\boldsymbol{v}_{y2'} + l_6\cdot\Delta\boldsymbol{v}_{z2'} \\ &= \frac{2i_{21}\cdot l_4 l_7}{3}\left[-\sqrt[3]{\frac{M_1^2 l_4^2}{k^2m^2R^5}}\left(\frac{l_{Ru}l_{13}}{l_{14}} + \frac{l_{Rv}l_{11}}{l_{12}}\right) + \sqrt[3]{\frac{M_1^2}{k^2m^2R^2l_4}}\left(\frac{l_{4u}l_{13}}{l_{14}} + \frac{l_{4v}l_{11}}{l_{12}}\right)\right] \\ &\quad + \frac{2i_{21}\cdot l_5 l_7}{3}\left[-\sqrt[3]{\frac{M_1^2 l_5^2}{k^2m^2R^5}}\left(\frac{l_{Ru}l_{13}}{l_{14}} + \frac{l_{Rv}l_{11}}{l_{12}}\right) + \sqrt[3]{\frac{M_1^2}{k^2m^2R^2l_5}}\left(\frac{l_{5u}l_{13}}{l_{14}} + \frac{l_{5v}l_{11}}{l_{12}}\right)\right] \\ &\quad + \frac{2i_{21}\cdot l_6 l_7}{3}\left[-\sqrt[3]{\frac{M_1^2 l_6^2}{k^2m^2R^5}}\left(\frac{l_{Ru}l_{13}}{l_{14}} + \frac{l_{Rv}l_{11}}{l_{12}}\right) + \sqrt[3]{\frac{M_1^2}{k^2m^2R^2l_6}}\left(\frac{l_{6u}l_{13}}{l_{14}} + \frac{l_{6v}l_{11}}{l_{12}}\right)\right] \end{aligned} \tag{38}$$

B. CONJUGATE EQUATION WITH ELASTIC DEFORMATION BETWEEN THE STATIONARY INTERNAL TOROIDAL GEAR AND PLANET-WORM GEAR

The meshing condition between a planet-worm gear and stationary internal toroidal gear is the same as that between a planet-worm gear and sun-worm. Taking the same steps, the elastic meshing equation and elastic meshing function of conjugate surfaces $\sum(2)$ and $\sum(3)$ can be derived in $\mathbf{S}_{2'}$ as:

$$\begin{cases} \sin(\alpha' + u) = \dfrac{-l_{18}\cos v - l_{22}}{\sqrt{l_{19}^2 + l_{20}^2}\sin v} \\ \Phi_{23} = \boldsymbol{n}_{2'}\cdot\boldsymbol{v}_0^{(2'3')} = l_{18}\cos v + l_{19}\cos u\sin v \\ \qquad + l_{20}\sin u\sin v + l_{22} \end{cases} \tag{39}$$

where,

$$\begin{aligned} l_{22} &= \boldsymbol{n}_{2'}\cdot\frac{d\boldsymbol{\delta}^{(2'3')}}{dt} \\ &= \frac{2i_{23}\cdot l_4 l_{7'}}{3}\left[-\sqrt[3]{\frac{M_3^2 l_4^2}{k^2n^2R'^5}}\left(\frac{l_{R'u}l_{13'}}{l_{14'}} + \frac{l_{R'v}l_{11'}}{l_{12'}}\right) + \sqrt[3]{\frac{M_3^2}{k^2n^2R'^2l_4}}\left(\frac{l_{4u}l_{13'}}{l_{14'}} + \frac{l_{4v}l_{11'}}{l_{12'}}\right)\right] \\ &\quad + \frac{2i_{23}\cdot l_5 l_{7'}}{3}\left[-\sqrt[3]{\frac{M_3^2 l_5^2}{k^2n^2R'^5}}\left(\frac{l_{R'u}l_{13'}}{l_{14'}} + \frac{l_{R'v}l_{11'}}{l_{12'}}\right) + \sqrt[3]{\frac{M_3^2}{k^2n^2R'^2l_5}}\left(\frac{l_{5u}l_{13'}}{l_{14'}} + \frac{l_{5v}l_{11'}}{l_{12'}}\right)\right] \\ &\quad + \frac{2i_{23}\cdot l_6 l_{7'}}{3}\left[-\sqrt[3]{\frac{M_3^2 l_6^2}{k^2n^2R'^5}}\left(\frac{l_{R'u}l_{13'}}{l_{14'}} + \frac{l_{R'v}l_{11'}}{l_{12'}}\right) + \sqrt[3]{\frac{M_3^2}{k^2n^2R'^2l_6}}\left(\frac{l_{6u}l_{13'}}{l_{14'}} + \frac{l_{6v}l_{11'}}{l_{12'}}\right)\right] \end{aligned} \tag{40}$$

M_3 is the torque of the stationary internal gear.

C. INSTANTANEOUS CONTACT EQUATION WITH ELASTIC DEFORMATION

The instantaneous contact curve equation on the planet worm-gear tooth between the planet-worm gear and sun-worm is:

$$\begin{cases} x_{2'} = \rho\cos v + r_2 \\ y_{2'} = \rho\cos u\sin v \\ z_{2'} = \rho\sin u\sin v \\ \sin(\alpha+u) = \dfrac{-l_8\cos v - l_{21}}{\sqrt{l_9^2+l_{10}^2}\sin v} \end{cases} \tag{41}$$

Similarly, the instantaneous contact curve equation on the planet worm-gear tooth between the planet-worm gear and stationary internal toroidal gear is:

$$\begin{cases} x_{2'} = \rho\cos v + r_2 \\ y_{2'} = \rho\cos u\sin v \\ z_{2'} = \rho\sin u\sin v \\ \sin(\alpha'+u) = \dfrac{-l_{18}\cos v - l_{22}}{\sqrt{l_{19}^2+l_{20}^2}\sin v} \end{cases} \tag{42}$$

D. INDUCED NORMAL CURVATURE EQUATION WITH ELASTIC DEFORMATION

1) FIRST BOUNDARY CURVE FUNCTION

Based on the gear meshing theory, the first boundary curve function for meshing between a planet-worm gear and sun-worm can be expressed:

$$\boldsymbol{\Psi}_{21} = \frac{1}{D_2^2}\begin{vmatrix} E_2 & F_2 & \boldsymbol{r}_{2'(u)}\cdot\boldsymbol{v}^{(2'1')} \\ F_2 & G_2 & \boldsymbol{r}_{2'(v)}\cdot\boldsymbol{v}^{(2'1')} \\ \boldsymbol{\Phi}_{21(u)} & \boldsymbol{\Phi}_{21(v)} & \boldsymbol{\Phi}_{21(t)} \end{vmatrix} \tag{43}$$

where $\boldsymbol{v}^{(2'1')}$ is the same as Eq. (11), $\boldsymbol{r}_{2'(u)}$, $\boldsymbol{r}_{2'(v)}$, $\boldsymbol{\Phi}_{21(u)}$, $\Phi_{21(v)}$ and $\Phi_{21(t)}$ can be derived by taking the derivative of Eq. (1) and Eq. (37) with respect to meshing parameters u, v and time t.

The other elements in Eq. (43) are represented as follows:

$$\begin{cases} E_2 = (\boldsymbol{r}_{2'(u)})^2 = \rho^2\sin^2 v \\ F_2 = (\boldsymbol{r}_{2'(u)}\cdot\boldsymbol{r}_{2'(v)}) = 0 \\ G_2 = (\boldsymbol{r}_{2'(v)})^2 = \rho^2 \\ D_2^2 = E_2G_2 - F_2 = \rho^4\sin^2 v \end{cases} \tag{44}$$

Through calculation, the following equations can be obtained (45), as shown at the top of the next page.

Then, the first boundary curve function for meshing between a planet-worm gear and sun-worm can be represented:

$$\begin{cases} x_{1'} = \cos\varphi_1\cos\varphi_2 x_{2'} - \cos\varphi_1\sin\varphi_2 y_{2'} \\ \quad -\sin\varphi_1 z_{2'} + a_0\cos\varphi_1 \\ y_{1'} = -\sin\varphi_1\cos\varphi_2 x_{2'} + \sin\varphi_1\sin\varphi_2 y_{2'} \\ \quad -\cos\varphi_1 z_{2'} - a_0\sin\varphi_1 \\ z_{1'} = \sin\varphi_2 x_{2'} + \cos\varphi_2 y_{2'} \\ \sin(\alpha+u) = -(l_8\cos v + l_{21})\Big/\sqrt{l_9^2+l_{10}^2}\sin v \\ \boldsymbol{\Psi}_{21} = 0 \end{cases} \tag{46}$$

Taking the same steps, the first boundary curve equation for meshing between a planet-worm gear and stationary internal toroidal gear is represented as follows:

$$\begin{cases} x_{3'} = \cos\varphi_3\cos\varphi_2 x_{2'} - \cos\varphi_3\sin\varphi_2 y_{2'} \\ \quad -\sin\varphi_3 z_{2'} + a_0\cos\varphi_3 \\ y_{3'} = -\sin\varphi_3\cos\varphi_2 x_{2'} + \sin\varphi_3\sin\varphi_2 y_{2'} \\ \quad -\cos\varphi_3 z_{2'} - a_0\sin\varphi_3 \\ z_{3'} = \sin\varphi_2 x_{2'} + \cos\varphi_2 y_{2'} \\ \sin(\alpha'+u) = -(l_{18}\cos v + l_{22})\Big/\sqrt{l_{19}^2+l_{20}^2}\sin v \\ \Psi_{23} = 0 \end{cases} \tag{47}$$

2) SECOND BOUNDARY CURVE FUNCTION

When the toroidal drive works, not all of the points on the conjugate surfaces participate in the meshing process. In one instant, just one section of the tooth surface participates in the meshing process. The second boundary curve is the dividing line between the meshing zone and non-meshing zone. Based on the gear theory, function and equation of the second boundary curve between a planet-worm gear and sun-worm are as follows:

$$\begin{cases} \boldsymbol{r}_{2'} = \boldsymbol{r}_{2'}(u,v) \\ \Phi_{21}(u,v,t) = 0 \\ \Phi_{21\,(t)}(u,v,t) = 0 \end{cases} \tag{48}$$

That is:

$$\begin{cases} x_{2'} = \rho\cos v + r_2 \\ y_{2'} = \rho\cos u\sin v \\ z_{2'} = \rho\sin u\sin v \\ \sin(\alpha+u) = -(l_8\cos v + l_{21})\Big/\sqrt{l_9^2+l_{10}^2}\sin v \\ -\boldsymbol{\omega}_2 r_2\sin\varphi_2\sin u\sin v + l_{21(t)} = 0 \end{cases} \tag{49}$$

The second boundary curve function between a planet-worm gear and stationary internal toroidal gear can be expressed as follows:

$$\begin{cases} x_{2'} = \rho\cos v + r_2 \\ y_{2'} = \rho\cos u\sin v \\ z_{2'} = \rho\sin u\sin v \\ \sin(\alpha'+u) = -(l_{18}\cos v + l_{22})\Big/\sqrt{l_{19}^2+l_{20}^2}\sin v \\ -\boldsymbol{\omega}_2 r_2\sin\varphi_2\sin u\sin v + l_{22(t)} = 0 \end{cases} \tag{50}$$

$$\begin{cases} \boldsymbol{r}_{2'(u)} \cdot \boldsymbol{v}^{(2'1')} = \rho^2 \sin v(\cos\varphi_2 \cos u \cos v - \sin\varphi_2 \sin v - i_{21} \sin u \cos v) \\ \qquad + \rho \sin v[r_2 \cos\varphi_2 \cos u - i_{21} \cdot r_2 \sin u + \Delta v_{y2'} \sin u + (a_0 + \Delta v_{z2'}) \cos u] \\ \boldsymbol{r}_{2'(v)} \cdot \boldsymbol{v}^{(2'1')} = \rho^2(\cos\varphi_2 \sin u + i_{21} \cos u) + \rho[i_{21} \cdot r_2 \cos u \cos v + r_2 \cos\varphi_2 \sin u \cos v \\ \qquad - \Delta v_{x2'} \sin v + \Delta v_{y2'} \cos u \cos v + (a_0 + \Delta v_{y2'}) \sin u \cos v] \end{cases} \tag{45}$$

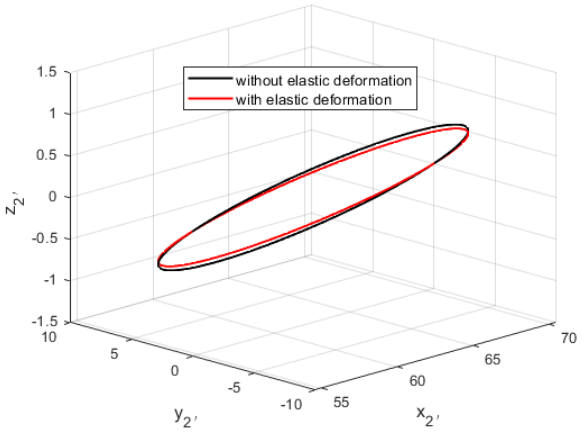

(a)

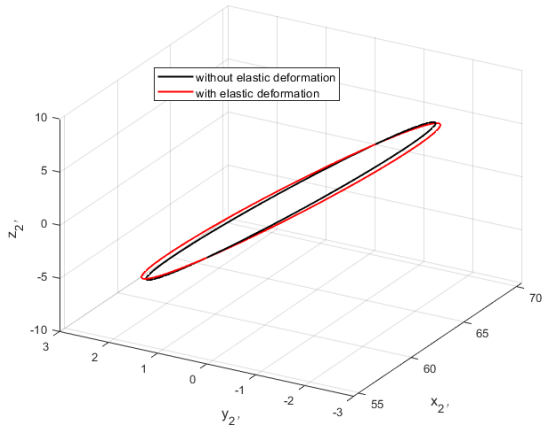

(b)

FIGURE 11. (a). Contact curve influenced by elastic deformation between $\sum(2)$ and $\sum(1)$. (b). Contact curve influenced by elastic deformation between $\sum(2)$ and $\sum(3)$.

3) INDUCED NORMAL CURVATURE

Based on the gear meshing theory, the induced normal curvatures between a planet-worm gear and sun-worm and that between a planet-worm gear and stationary internal toroidal gear are represented in Eq. (51) and Eq. (52) respectively.

$$K_\sigma^{(2'1')} = \frac{1}{D_2^2 \boldsymbol{\Psi}_{21}}(E_2 \boldsymbol{\Phi}_{21(u)}^2 - 2F_2 \boldsymbol{\Phi}_{21(u)} \boldsymbol{\Phi}_{21(v)} + G_2 \boldsymbol{\Phi}_{21(v)}^2) \tag{51}$$

$$K_\sigma^{(2'3')} = \frac{1}{D_2^2 \boldsymbol{\Psi}_{23}}(E_2 \boldsymbol{\Phi}_{23(u)}^2 - 2F_2 \boldsymbol{\Phi}_{23(u)} \boldsymbol{\Phi}_{23(v)} + G_2 \boldsymbol{\Phi}_{23(v)}^2) \tag{52}$$

E. HELIX-LEAD ANGLE EQUATION OF THE SUN-WORM AND STATIONARY INTERNAL TOROIDAL GEAR

1) HELIX-LEAD ANGLE EQUATION OF THE SUN-WORM

According to the solving process of helix-lead angle [2], this paper only gives the final helix-lead angle expression involving the influence of elastic deformation.

$$\lambda_1 = \arccos \frac{\sqrt{A_1^2 + B_1^2}}{\sqrt{A_1^2 + B_1^2 + C_1^2}} \tag{53}$$

where,

$$\begin{cases} A_1 = (n_{y1'} n_{bz1'} - n_{z1'} n_{by1'}) \\ B_1 = (n_{z1'} n_{bx1'} - n_{x1'} n_{bz1'}) \\ C_1 = (n_{x1'} n_{by1'} - n_{y1'} n_{bx1'}) \\ n_{bx1'} = x_{1'}[1 - a_0 \Big/ \sqrt{x_{1'}^2 + y_{1'}^2}] \\ n_{by1'} = y_{1'}[1 - a_0 \Big/ \sqrt{x_{1'}^2 + y_{1'}^2}] \\ n_{bz1'} = z_{1'} \\ n_{x1'} = \cos\varphi_1 \cos\varphi_2 n_{x2'} - \cos\varphi_1 \sin\varphi_2 n_{y2'} - \sin\varphi_1 n_{z2'} \\ n_{y1'} = -\sin\varphi_1 \cos\varphi_2 n_{x2'} + \sin\varphi_1 \sin\varphi_2 n_{y2'} - \cos\varphi_1 n_{z2'} \\ n_{z1'} = \sin\varphi_2 n_{x2'} + \cos\varphi_2 n_{y2'} \end{cases} \tag{54}$$

2) HELIX-LEAD ANGLE EQUATION OF THE STATIONARY INTERNAL TOROIDAL GEAR

Similarly, helix-lead angle of the stationary internal toroidal gear can be expressed as follows:

$$\lambda_3 = \arccos \frac{\sqrt{A_3^2 + B_3^2}}{\sqrt{A_3^2 + B_3^2 + C_3^2}} \tag{55}$$

where,

$$\begin{cases} A_3 = (n_{y3'} n_{bz3'} - n_{z3'} n_{by3'}) \\ B_3 = (n_{z3'} n_{bx3'} - n_{x3'} n_{bz3'}) \\ C_3 = (n_{x3'} n_{by3'} - n_{y3'} n_{bx3'}) \\ n_{bx3'} = x_{3'}[1 - a_0 \Big/ \sqrt{x_{3'}^2 + y_{3'}^2}] \\ n_{by3'} = y_{3'}[1 - a_0 \Big/ \sqrt{x_{3'}^2 + y_{3'}^2}] \\ n_{bz3'} = z_{3'} \\ n_{x3'} = \cos\varphi_3 \cos\varphi_2 n_{x2'} - \cos\varphi_3 \sin\varphi_2 n_{y2'} - \sin\varphi_3 n_{z2'} \\ n_{y3'} = -\sin\varphi_3 \cos\varphi_2 n_{x2'} + \sin\varphi_3 \sin\varphi_2 n_{y2'} - \cos\varphi_3 n_{z2'} \\ n_{z3'} = \sin\varphi_2 n_{x2'} + \cos\varphi_2 n_{y2'} \end{cases} \tag{56}$$

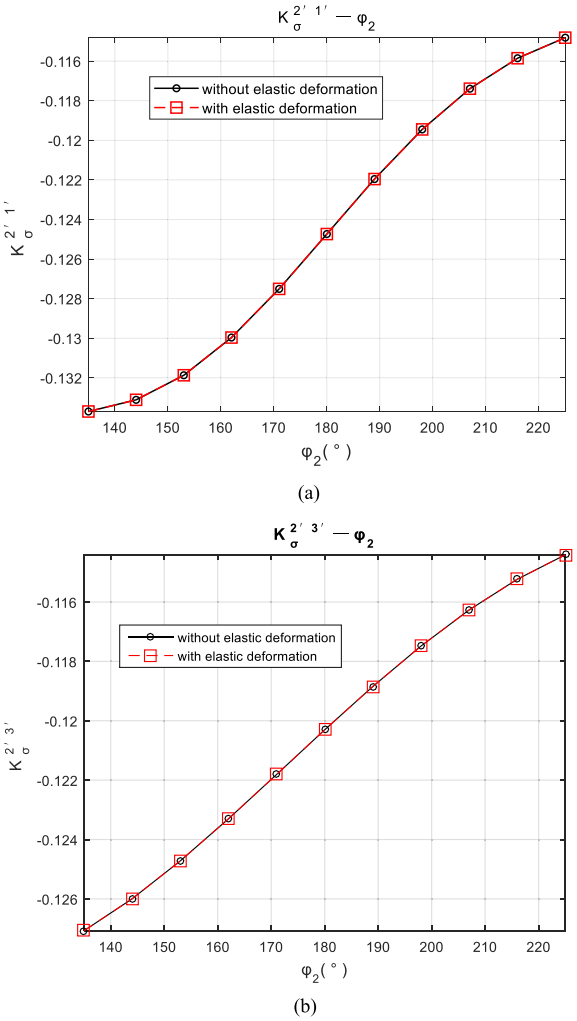

FIGURE 12. (a). Induced normal curvature between a planet worm-gear and sun-worm influenced by elastic deformation. (b). Induced normal curvature between a planet worm-gear and stationary internal toroidal gear influenced by elastic deformation.

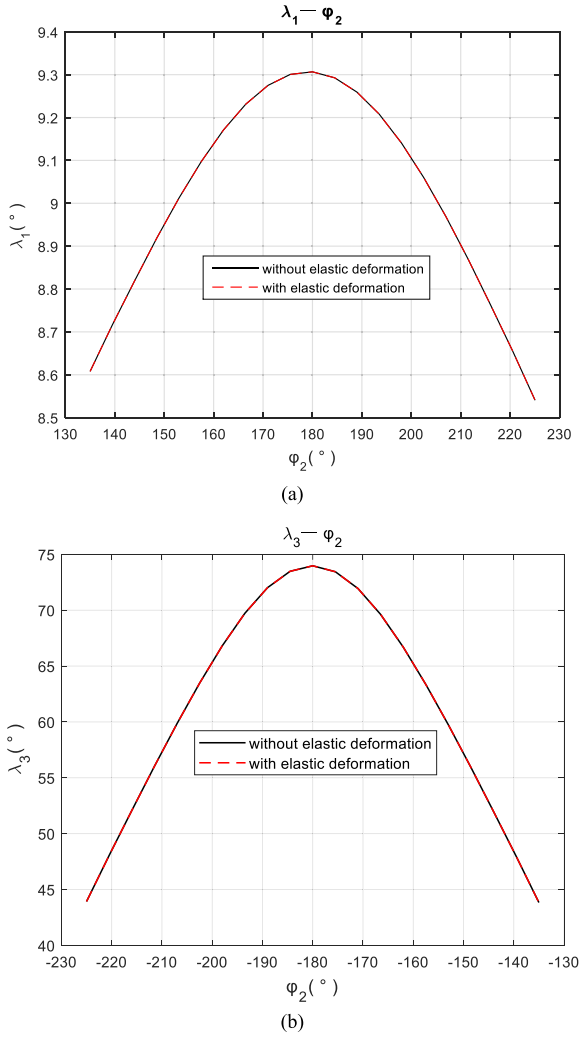

FIGURE 13. (a). The helix-lead angle of the sun-worm influenced by elastic deformation. (b). The helix-lead angle of the stationary internal gear influenced by elastic deformation.

V. ELASTIC DEFORMATION INFLUENCE ON THE MESHING CHARACTERISTIC OF THE TOROIDAL DRIVE

According to equations deduced above, the meshing contact curve as well as induced normal curvature curve and helix-lead angle curve with elastic deformation can be obtained. The influence of elastic deformation on meshing performance can be investigated by comparing the curves with and without elastic deformation.

A. ELASTIC DEFORMATION INFLUENCE ON THE MESHING CONTACT CURVE

The contact curve on the planet-worm gear tooth surface between the planet-worm gear and sun-worm is given by Eq. (41), and that between the planet-worm gear and internal toroidal gear is determined by Eq. (42). The elastic deformation influence on the contact curve between conjugate surfaces $\sum(1)$ and $\sum(2)$, as well as between $\sum(2)$ and $\sum(3)$, are shown in Fig. 11 (a) and (b). The meshing contact curve without elastic deformation is given in the figure as a reference. It can be found in the figures that the elastic deformation has a little effect on contact curve which induce the contact curve rotates a very small angle about a certain axis.

B. ELASTIC DEFORMATION INFLUENCE ON THE INDUCED NORMAL CURVATURE

The induced normal curvature of the meshing between the planet-worm gear and sun-worm, and that between the planet-worm gear and stationary internal toroidal gear are represented in Eq. (51) and Eq. (52). Fig. 12(a) and (b) show the effect of elastic deformation on the induced normal curvatures. It can be observed that the induced normal curvature $K_\sigma^{2'1'}$ and $K_{\sigma 2'3'}$ are hardly affected by elastic deformation.

C. ELASTIC DEFORMATION INFLUENCE ON THE HELIX-LEAD ANGLE

The helix-lead angle of the sun-worm and stationary internal toroidal gear are important in the manufacturing and assembly process of the toroidal drive. The helix-lead angle is not

constant but varies with the changing of the planet-worm gear rotation angle φ_2.

The helix-lead angle of the sun-worm and internal toroidal gear are determined by Eq. (53) and Eq. (55), respectively. The elastic deformation influence on the helix-lead angle λ_1 and λ_3 are shown in Fig. 13(a) and (b), respectively. It is obviously that the helix-lead angle λ_1 and λ_3 are hardly affected by elastic deformation.

VI. CONCLUSION

Elastic deformation in the rolling contact process is one of the main reasons for the time-varying mesh stiffness of the toroidal drive. In this paper, an elastic deformation mathematical model based on Wills law and Hertz contact theory is proposed, which can be used as a theoretical basis for toroidal drive regarding the vibration and noise analysis. The main works accomplished are as follows:

1. Elastic deformation integrated coordinate systems are built to describe the position relationship among the main components of the toroidal drive.
2. According to Hertz contact theory, the relationship between elastic deformation velocity and normal force at contact point is studied. The elastic deformation velocity induced by contact force is adopted for the first time in the relative velocity of the Wills law for the toroidal drive.
3. Elastic conjugate equations between the sun-worm and planet-worm gear as well as between the stationary internal toroidal gear and planet-worm gear are induced. The influences of elastic deformation on the meshing contact curves, helix-lead angle and induced normal curvature of toroidal drive are discussed. The results indicate that: (1) Elastic deformation has a little effect on contact curve, which is rotated by a very small angle about a certain axis. (2) Induced normal curvature and helix-lead angle are hardly affected by elastic deformation.

NOMENCLATURE

$\boldsymbol{S}_0(O_0, \boldsymbol{i}_0, \boldsymbol{j}_0, \boldsymbol{k}_0)$	reference coordinate system of the meshing roller
$\boldsymbol{S}_{0'}(O_{0'}, \boldsymbol{i}_{0'}, \boldsymbol{j}_{0'}, \boldsymbol{k}_{0'})$	movable coordinate system of the meshing roller
$\boldsymbol{S}_1(O_1, \boldsymbol{i}_1, \boldsymbol{j}_1, \boldsymbol{k}_1)$	reference coordinate system of the sun-worm
$\boldsymbol{S}_{1'}(O_{1'}, \boldsymbol{i}_{1'}, \boldsymbol{j}_{1'}, \boldsymbol{k}_{1'})$	movable coordinate system of the sun-worm
$\boldsymbol{S}_2(O_2, \boldsymbol{i}_2, \boldsymbol{j}_2, \boldsymbol{k}_2)$	reference coordinate system of the planet-worm gear
$\boldsymbol{S}_{2'}(O_{2'}, \boldsymbol{i}_{2'}, \boldsymbol{j}_{2'}, \boldsymbol{k}_{2'})$	movable coordinate system of the planet-worm gear
$\boldsymbol{S}_3(O_3, \boldsymbol{i}_3, \boldsymbol{j}_3, \boldsymbol{k}_3)$	reference coordinate system of the internal toroidal gear
$\boldsymbol{\omega}_1$	angular velocity of the sun-worm
$\boldsymbol{\omega}_2$	angular velocity of the planet-worm gear
$\boldsymbol{\varphi}_1$	rotation angle of the sun-worm about $k_{1'}$
$\boldsymbol{\varphi}_2$	rotation angle of the planet-worm gear about $k_{2'}$
$\Sigma(1)$	tooth surface of the sun-worm
$\Sigma(2)$	tooth surface of the planet-worm gear
$\Sigma(3)$	tooth surface of the stationary internal toroidal gear
$\boldsymbol{\xi}$	$\overrightarrow{O_{1'}O_{2'}}$
P	meshing contact point between the meshing roller and sun-worm
$\boldsymbol{r}_{2'}$	vector of the meshing roller in $\boldsymbol{S}_{2'}$
$\boldsymbol{r}_0$	vector of the meshing roller in $\boldsymbol{S}_0$
ρ	radius of the meshing roller
r_2	radius of the planet-worm gear
u	spherical parameter of meshing roller
v	spherical parameter of meshing roller
$M_{2'0}$	coordinate transformation matrix from $\boldsymbol{S}_0$ to $\boldsymbol{S}_{2'}$
$\boldsymbol{n}2'$	unit normal vector of contact point P in $\boldsymbol{S}_{2'}$
$\boldsymbol{v}^{(2'1')}$	relative velocity between the planet-worm gear and sun-worm
i_{21}	transmission ratio between the planet-worm gear and sun-worm
$\boldsymbol{\omega}^{(2'1')}$	relative angular velocity between the planet-worm gear and sun-worm
a_0	central distance of the toroidal drive
$\boldsymbol{\delta}^{(2'1')}$	elastic deformation between the sun-worm and planet-worm gear
$d\boldsymbol{\delta}_{\xi}^{(2'1')}/dt$	elastic deformation velocity along the direction of $O_{1'}O_{2'}$
$d\boldsymbol{\delta}^{(2'1')}/dt$	elastic deformation velocity along the translocation direction of the contact surface between the sun-worm and planet-worm gear
$(x_{2'}, y_{2'}, z_{2'})$	coordinate components of the roller profile in $\boldsymbol{S}_{2'}$
$(\Delta v_{x2'}, \Delta v_{y2'}, \Delta v_{z2'})$	variations of the relative velocities
$\boldsymbol{P}_1$	normal force at point P
P_1	module of normal force $\boldsymbol{P}_1$
$\boldsymbol{r}_P$	radius vector of the sun-worm at contact point P
$\boldsymbol{F}_{t1}$	driving force between the sun-worm and planet-worm gear
$\boldsymbol{F}_{a1}$	axial force between the sun-worm and planet-worm gear

$\boldsymbol{F}_{r1}$	radial force between the sun-worm and planet-worm gear
$\boldsymbol{F}'_{t1}$	reaction force of $\boldsymbol{F}_{t1}$
$\boldsymbol{F}'_{a1}$	reaction force of $\boldsymbol{F}_{a1}$
$\boldsymbol{F}'_{r1}$	reaction force of $\boldsymbol{F}_{r1}$
$\boldsymbol{F}_{t3}$	driving force between the internal toroidal gear and planet-worm gear
$\boldsymbol{F}_{a3}$	axial force between the internal toroidal gear and planet-worm gear
$\boldsymbol{F}_{r3}$	radial force between the internal toroidal gear and planet-worm gear
$\boldsymbol{F}'_{t3}$	reaction force of $\boldsymbol{F}_{t3}$
$\boldsymbol{F}'_{a3}$	reaction force of $\boldsymbol{F}_{a3}$
$\boldsymbol{F}'_{r3}$	reaction force of $\boldsymbol{F}_{r3}$
$\boldsymbol{M}_1$	torque of the sun-worm
m	meshing point number between the sun-worm and planet-worm gears
n	meshing point number between the internal toroidal gear and planet-worm gears
k	number of planet-worm gears
a_{12}	value of major half-axis of the elliptical contact region
b_{12}	value of the minor half-axis of the elliptical contact region
α_{12}	interpolation coefficient
β_{12}	interpolation coefficient
m_{12}	geometry parameters of the contact ellipse
n_{12}	geometry parameters of the contact ellipse
μ_1	Poisson's ratio of the material of the sun-worm
μ_2	Poisson's ratio of the material of the meshing roller
ρ_{11}	curvatures of the sun-worm tooth and meshing roller
ρ_{12}	curvatures of the sun-worm tooth and meshing roller
ρ_{21}	curvatures of the sun-worm tooth and meshing roller
ρ_{22}	curvatures of the sun-worm tooth and meshing roller
J_{12}	elliptic integral parameter
J_{12}/α_{12}	elliptic integral parameter
$\boldsymbol{r}_{2'(u)}$	derivative of $\boldsymbol{r}_{2'}$ with respect to u
$\boldsymbol{r}_{2'(v)}$	derivative of $\boldsymbol{r}_{2'}$ with respect to v
$\boldsymbol{\Phi}_{21}$	meshing function between the sun-worm and planet-worm gear
$\boldsymbol{\Phi}_{21(u)}$	derivative of $\boldsymbol{\Phi}_{21}$ with respect to u
$\boldsymbol{\Phi}_{21(v)}$	derivative of $\boldsymbol{\Phi}_{21}$ with respect to v
$\boldsymbol{\Phi}_{21(t)}$	derivative of $\boldsymbol{\Phi}_{21}$ with respect to t
$\boldsymbol{\Phi}_{23}$	meshing function between the internal toroidal gear and planet-worm gear
$\boldsymbol{\Phi}_{23(u)}$	derivative of $\boldsymbol{\Phi}_{23}$ with respect to u
$\boldsymbol{\Phi}_{23(v)}$	derivative of $\boldsymbol{\Phi}_{23}$ with respect to v
$\boldsymbol{\Phi}_{23(t)}$	derivative of $\boldsymbol{\Phi}_{23}$ with respect to t
$\boldsymbol{\Psi}_{21}$	first boundary curve function between a planet-worm gear and sun-worm
$\boldsymbol{\Psi}_{23}$	first boundary curve function between a planet-worm gear and internal toroidal gear
$K_{\sigma}^{(2'1')}$	induced normal curvature between a planet-worm gear and sun-worm
$K_{\sigma}^{(2'3')}$	induced normal curvature between a planet-worm gear and internal toroidal gear
λ_1	helix-lead angle of the sun-worm
λ_3	helix-lead angle of the internal toroidal gear

REFERENCES

[1] M. R. Kuehnle, "Toroidal transmission," Patents 1 301 682, Aug. 21, 1969.
[2] L. Yao, J. S. Dai, G. Wei, and H. Li, "Geometric modeling and meshing characteristics of the toroidal drive," *J. Mech. Des.*, vol. 127, no. 5, pp. 988–996, 2005.
[3] L. Yao, J. S. Dai, G. Wei, and Y. Cai, "Comparative analysis of meshing characteristics with respect to different meshing rollers of the toroidal drive," *Mechanism Mach. Theory*, vol. 41, no. 7, pp. 863–881, 2006.
[4] H. Peeken, "Berechnung und messung der lastverteilung im Toroidgeriebe," *Konstruktion*, vol. 36, no. 3, pp. 81–86, 1984.
[5] L. Xu and Z. Huang, "Modelling and simulation of friction for toroidal drive," *Proc. Inst. Mech. Eng. J, J. Eng. Tribol.*, vol. 221, no. 1, pp. 75–84, 2007.
[6] L. Xu and Z. Huang, "Wear calculation for toroidal drive," *J. Mech. Des.*, vol. 128, no. 4, pp. 820–823, 2006.
[7] L. Yao, J. S. Dai, and H. Li, "Mathematical modelling and manufacturing of the internal toroidal tooth profile," *Proc. Inst. Mech. Eng. C, J. Mech. Eng. Sci.*, vol. 218, pp. 1043–1051, Sep. 2004.
[8] L. Yao, G. W. Wei, Z. H. Lan, and J. S. Dai, "Comparative study on machining the internal stationary toroidal gear," *Key Eng. Mater.*, vols. 291–292, pp. 483–488, Aug. 2005.
[9] W. Mo, Y. Jiao, and Z. Chen, "Dynamic analysis of helical gears with sliding friction and gear errors," *IEEE ACCESS*, vol. 6, pp. 60467–60477, 2018.
[10] Y. Sun, H. Ma, Y. Huangfu, K. Chen, L. Che, and B. Wen, "A revised time-varying mesh stiffness model of spur gear pairs with tooth modifications," *Mech. Mach. Theory*, vol. 129, pp. 261–278, Nov. 2018.
[11] C. G. Cooley, C. Liu, X. Dai, and R. G. Parker, "Gear tooth mesh stiffness: A comparison of calculation approaches," *Mech. Mach. Theory*, vol. 105, pp. 540–553, Nov. 2016.
[12] J.-F. Shi, X.-F. Gou, and L.-Y. Zhu, "Modeling and analysis of a spur gear pair considering multi-state mesh with time-varying parameters and backlash," *Mech. Mach. Theory*, vol. 134, pp. 582–603, Apr. 2019.
[13] H. Ma, J. Zeng, R. Feng, X. Pang, and B. Wen, "An improved analytical method for mesh stiffness calculation of spur gears with tip relief," *Mech. Mach. Theory*, vol. 98, pp. 64–80, Apr. 2016.
[14] P.-Y. Wang, S.-C. Fan, and Z.-G. Huang, "Spiral bevel gear dynamic contact and tooth impact analysis," *J. Mech. Des.*, vol. 133, no. 8, 2011, Art. no. 084501.
[15] C. Lin and Z. Cai, "Research on the method to calculate deformation of curve-face gear," *Proc. Inst. Mech. Eng. C, J. Mech. Eng. Sci.*, vol. 232, no. 13, pp. 2458–2468, 2018.
[16] Z. Chen and Y. Shao, "Mesh stiffness of an internal spur gear pair with ring gear rim deformation," *Mech. Mach. Theory*, vol. 69, pp. 1–12, Nov. 2013.
[17] M. Ajmi and P. Velex, "A model for simulating the quasi-static and dynamic behaviour of solid wide-faced spur and helical gears," *Mech. Mach. Theory*, vol. 40, no. 2, pp. 173–190, 2005.
[18] L. Chang, G. Liu, and L. Wu, "A robust model for determining the mesh stiffness of cylindrical gears," *Mech. Mach. Theory*, vol. 87, pp. 93–114, May 2015.
[19] M. B. Sánchez, M. Pleguezuelos, and J. I. Pedrero, "Approximate equations for the meshing stiffness and the load sharing ratio of spur gears including hertzian effects," *Mech. Mach. Theory*, vol. 109, pp. 231–249, Mar. 2017.

[20] F. G. Nakhatakyan, "Determining the flexural stress concentration factor for gear teeth taking into account elastic deformations and errors in manufacture and assembly of gearing elements," *J. Machinery Manuf. Rel.*, vol. 37, no. 4, pp. 348–351, 2008.
[21] S. Ebrahimi and P. Eberhard, "Rigid-elastic modeling of meshing gear wheels in multibody systems," *Multibody Syst. Dyn.*, vol. 16, pp. 55–71, Aug. 2006.
[22] C. Hu, X. Tang, L. Zou, K. Yang, Y. Li, and L. Zheng, "Numerical and experimental investigations of noise and vibration characteristics for a dual-motor hybrid electric vehicle," *IEEE Access*, vol. 7, pp. 77052–77062, 2019.
[23] F. L. Litvin and A. Fuentes, *Gear Geometry and Applied Theory*. Cambridge, U.K.: Cambridge Univ. Press, 2004.

XUELIAN ZENG received the M.S. degree in mechanical design and theory from Fuzhou University, Fuzhou, China, in 2012, where she is currently pursuing the Ph.D. degree with the Mechanical Engineering and Automation School. She is also a Lecturer of Fujian Chuanzheng Communications College. Her current research interests include kinematics analysis, complex surface modeling, and precision manufacturing.

LIGANG YAO received the Ph.D. degree in mechanical engineering from the Harbin Institute of Technology, China, in 1996.

He is currently the Director of the Gear Lab, Fuzhou University, where he is also a Professor with the School of Mechanical Engineering and Automation. He has published more than 70 international journal articles. His research interests include robot mechanism and mechanical transmission, rehabilitation robot, modern design method, complex surface modeling, and precision manufacturing. He is also a member of the ASME and a Senior Member of the Chinese Mechanical Engineering Society. He has served as a Reviewer of related journals for years.

JUN ZHANG received the B.S., M.S., and Ph.D. degrees from Tianjin University, China, in 2002, 2004, and 2007, respectively.

He is currently the Deputy Director of the Gear Lab, Fuzhou University, where he is also the Chair Professor with the School of Mechanical Engineering and Automation. He has published more than 30 international journal articles. His research interests include dynamic analysis, vibration control, and fault diagnosis. He has served as a Reviewer of related journals for years.

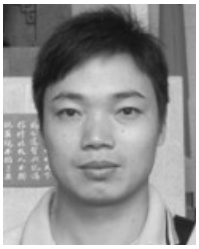

GUIYONG GUO received the M.S. degree in mechanical and electronic engineering from Fuzhou University, Fuzhou, China, in 2008, where he is currently pursuing the Ph.D. degree with the Mechanical Engineering and Automation School. His current research interests include signal and image processing and finite element analysis.

MEI HONG received the B.S., M.S., and Ph.D. degrees from Fuzhou University, China, in 2002, 2005, and 2014, respectively, where she is currently a Lecturer with the School of Mechanical Engineering and Automation. Her current research interests include dynamic analysis, digital design, and manufacture.